Proceedings of the 11th World Congress on Electrical Engineering and Computer Systems and Sciences (EECSS'25)
Paris, France - August, 2025
Paper No. ICBES 196
DOI: 10.11159/icbes25.196

Brain Response to Different Frequencies at the Action Potential and the effect of Sodium and Potassium Ratio on Neuron

Saeed Charbenny[1], Zhihong Huang[1]
[1]University of York
Heslington, York, United Kingdom
swd525@york.ac.uk; zhihong.huang@york.ac.uk

Abstract **-** Low-Intensity Focused Ultrasound (LIFU) shows promise as a non-invasive neuromodulation tool, yet its underlying mechanisms—thermal or mechanical—remain unclear. The link between LIFU exposure and action potential (AP) generation is not fully understood, and conventional thermal and mechanical detection lacks the sensitivity to capture subtle changes. This study uses simulation modeling to assess thermal and mechanical effects of different ultrasound frequencies at the AP threshold, aiming to clarify LIFU-induced neuromodulation mechanisms. This study simulates brain responses to LIFU at 0.250, 0.667, and 1 MHz frequencies, using AP threshold intensities. The goal is to investigate the frequency-dependent effects on brain thermal changes, displacement, force, and mechanical index (MI) at the AP threshold. A laboratory-based transducer was replicated in the simulation for validation, with thermal treatment modeled using a 50% duty cycle (DC) pulsed input. Brain temperature increased to 37.010704°C and 37.010708°C for 0.250 and 0.667 MHz, respectively, while 1 MHz resulted in a higher increase of 37.036869°C. Brain displacement values were 0.971 nm, 0.277 nm, and 0.227 nm for 0.250, 0.667, and 1 MHz, respectively. Force values were 0.03345, 0.15052, and 0.16376 N/m³ for 0.250, 0.667, and 1 MHz, respectively. MI decreased with increasing frequency, measuring 0.0138, 0.00867, and 0.00727 for 0.250, 0.667, and 1 MHz. Higher frequencies caused more significant temperature increases, especially at 1 MHz, where the focal thermal area was more concentrated compared to 0.250 and 0.667 MHz. Additionally, brain displacement decreased with frequency, and the MI also declined. While force and intensity increased with frequency, these results underscore the impact of frequency on brain interactions and suggest that neuron activation may be driven by thermal, mechanical, or combined energy mechanisms. Sodium and potassium ratio had an effect on whether neuron initiation could be achieved.

Keywords**:** Ultrasound, FUS, neuromodulation, thermal, neuron, action potential

1. Introduction

Non-invasive brain stimulation technologies have been limited by a lack of spatial precision comparable to invasive techniques. Transcranial magnetic stimulation (TMS) and transcranial electrical stimulation (TES) are two commonly used non-invasive methods. TMS has been shown to induce a tangential spread as small as 5 cm² and as large as 273 cm², with additional signal dispersion at greater depths [1]. TES, which delivers current between electrodes, results in widespread current distribution across non-targeted brain regions [2], [3]. Even with recent advancements in TES techniques [4], spatial selectivity remains limited. Focused ultrasound (FUS), a non-invasive neuromodulation technique, offers superior spatial resolution and penetration depth compared to both TES and TMS [5].

Focused ultrasound (FUS) neuromodulation is believed to exert its effects on neurons through two primary mechanisms: mechanical and thermal. The mechanical effects are thought to arise from voltage-driven imbalances in pressure between the extracellular and intracellular environments, leading to neuronal deformation. This deformation ultimately results in membrane displacement and structural shifts in the neuronal membrane [6], [7].

Although limited in number, existing studies suggest that thermal effects may play a significant role in FUS-induced neuromodulation. One study demonstrated reversible retroinhibition associated with a localized temperature increase of just 2 °C in the targeted area. These findings indicate that neural tissue is highly sensitive to even minimal elevations in temperature, supporting the potential role of thermal mechanisms in neuromodulation [8].

Simulations offer the ability to investigate neuronal and thermal responses to subtle perturbations, which are currently challenging to capture through experimental methods. The novelty of this study lies in its integration of single-neuron models using MetaNeuron [9], enabling an exploration of both mechanical and thermal effects on neuronal activation induced by a

focused acoustic beam. This is accomplished through Sim4Life [10], addressing the still-unclear mechanisms underlying ultrasound-neuron interactions.

2. Methods

2.1 Simulation of action potential

A neuron's action potential remains at a resting state in the absence of external stimulation. When subjected to a stimulus, the neuron may either become excited or inhibited, depending on the nature of the input. The transition from resting to active state is mediated by the exchange of sodium (Na^+) and potassium (K^+) ions, which initiates the depolarization phase. Successful neuronal activation is heavily dependent on reaching the threshold phase prior to depolarization—this threshold is essential for normal action potential initiation. The threshold and subsequent depolarization phases can be visualized using the classical model developed by Hodgkin, Huxley, and Katz [11]. In this study, we utilized the MetaNeuron software, which is capable of simulating action potentials and visualizing the effects of various stimuli on neuronal behaviour. To model normal conditions, the input parameters were set to a pulse width of 0.1 ms and an amplitude of 65 µA, as shown in Figure 1.

2.2. Transducer pressure and sensitivity recording

This study employed an experimental transducer setup to validate the outcomes of the simulation results. Sensitivity measurements were also necessary to convert neuronal voltage stimulation into equivalent acoustic pressure. The experimental setup included a 0.2-mm hydrophone needle, an amplifier, and a focused ultrasound (FUS) transducer (Precision Acoustics Ltd., Dorchester, Dorset, UK) with a resonance frequency of 667 kHz, an active diameter of 60 mm, and a focal length of 75 mm [12]. Focused pressure recordings were obtained by placing the ultrasound transducer in a water tank. The transducer was connected to a function generator (KEYSIGHT 33220A) and an RF power amplifier. The function generator output was set to 70 mV at a frequency of 667 kHz, which was subsequently amplified to 1 Watt. A 3D-axis positioning system was used to place the hydrophone at the transducer's focal point (75 mm). The hydrophone was connected to a DC coupler (DCPS160), which was interfaced with a PicoScope for data acquisition, visualization, and processing on a computer.

The conversion from voltage to pressure was by the following equation:

$$Pr = \frac{V}{S} \tag{1}$$

Where:
Pr: Is the acoustic pressure (Pascal)
V: is the output voltage of the hydrophone (Volt)
S: Sensitivity of the hydrophone (V/Pa)

2.3. Transducer simulation

Similar to the experimental setup, the simulation was conducted using a single-element ultrasound transducer modelled in Sim4Life simulation software (Sim4Life, Zurich, Switzerland). The transducer parameters included a curvature radius of 60 mm, an aperture width of 70 mm, and an operating frequency of 667 kHz.

2.4. Simulation setup

The simulated head model was imported from Sim4Life for the purpose of this study, with the focus of the simulation centred on the head region. The materials used in the simulation are detailed in Table 1. The head model represents a 34-year-old male, with a height of 1.77 m and a weight of 70.2 kg. The voxel resolution of the model consists of a pixel spacing of 0.5 × 0.5 mm and a slice thickness of 0.5 mm. The transducer was positioned on the upper right side of the head, above the right eye and ear. After preparing the simulation model, simulations were conducted using varying input parameters.

Table 1: Acoustic and thermal simulation material properties

Materials	Speed of sound m/s	Mass Density kg/m^3	Specific Heat Capacity J/kg/K	Thermal Conductivity W/m/K	Heat Generation Rate W/kg
Compact Skull	2813.69	1908	1312.83	0.32	0.154869
Cancellous skull	2117.53	1178.83	2274	0.3125	0.464607
Cerebrospinal fluid	1504.5	1007	4095.5	0.573333	0
Dura Matter	1500	1174	3364	0.44	5.88502
Brain (Grey matter)	1500	1044.5	3695.8	0.547	15.5391
Brain (White matter)	1552.5	1041	3582.8	0.481	4.32057
Commissura Anterior	1552.5	1041	3582.8	0.481	4.32057
Midbrain	1546.32	1045.5	3630	0.51325	11.3666
Thalamus	1500	1044.5	3695.8	0.547	13.9282
Pons	1546.32	1045.5	3630	0.51325	11.3666
Hypophysis	1500	1053	3687	0.514	13.7059
Hypothalamus	1500	1044.5	3695.8	0.547	15.5391
Hippocampus	1500	1044.5	3695.8	0.547	15.5391
Spinal Cord	1542	1075	3630	0.51325	2.48307
Cerebellum	1537	1045	3653	0.506	15.668
Medulla Oblongata	1546.32	1045.5	3630	0.51325	11.3666
Commissura Posterior	1552.5	1041	3582.8	0.481	4.32057
Pinal Body	1500	1053	3687	0.514	13.7059

2.5. Thermal simulation approach

Before conducting the simulation experiments specific to this study, we validated the simulation setup by replicating an existing therapeutic procedure. The referenced treatment utilized High Intensity Focused Ultrasound (HIFU) with an ultrasound power of 648 watts and a total energy delivery of 8,424 joules [14]. The simulation parameters were adjusted to match these conditions to ensure that the inputs used in our study accurately reflect the real-world settings typically encountered during therapeutic applications.

After confirming the treatment power and energy values, it was necessary to calculate the ultrasound intensity to accurately replicate it in the simulation. The intensity was determined using the following equation, which relates the treatment power to the spatial distribution of energy:

$$I = \frac{(P)}{(A)} \tag{2}$$

Where:
I: Is the intensity in Watt/m^2 or Watt/cm^2.
P: Is the power in Watt.
A: Is the transducer focused area in m^2 or cm^2.

Using Equation 2, the intensity of the treatment was calculated by first determining the area of the focused ultrasound beam. Since the exact focus area was not specified in the treatment, we approximated it based on the dimensions of the laboratory transducer. This approximation enabled the calculation of the ultrasound intensity, which was then matched within the simulation. The same simulation parameters were applied to estimate the pressure required to activate neuronal action

potentials. The HIFU treatment data was used solely to validate our simulation setup prior to conducting simulations of action potential (AP) activation thresholds.

Calculating the power or intensity required to activate the neuron was essential for the simulation. To achieve this, we utilized the MetaNeuron action potential voltage simulation model. This platform allowed us to visualize the neuronal response and determine the voltage threshold necessary for depolarization. Once the depolarization voltage was identified, it was converted into corresponding pressure and intensity values for use in the simulation. Using the first equation, which relates voltage to pressure, along with the known hydrophone sensitivity and target voltage, we calculated the pressure required to induce neuronal depolarization based on the action potential voltage.

After calculating the pressure required for neuronal activation, simulations were conducted to record the corresponding intensity based on the action potential threshold. Using the recorded power and intensity values, we determined the delivered energy parameters at the neuronal activation level. These pressure and intensity values were then used to simulate various frequencies with a 50% duty cycle to evaluate both the thermal effects and the mechanical index (MI) across different frequencies. This approach enables the assessment of thermal safety alongside mechanical effects during neuron activation.

Accuracy was ensured by aligning the thermal simulation with the parameters of the therapeutic treatment and validating the simulated thermal outputs against actual therapy data. Three different input signals were used, each consisting of sine-pulsed waves applied for 10 seconds. The sampling frequency was set at 5 MHz, with a pulse width of 5 ms.

As mechanical index depends on frequency, calculation are based on the given equation [13]:

$$MI = PNP/\sqrt{f} \tag{3}$$

Where:
MI: Is the mechanical index
PNP: Is the peak negative pressure in MPa
F: Excitation frequency in MHz

3. Results

3.1 Action potential and equilibrium

The resting membrane potential of the neuron was observed at –65 mV. Upon exposure to a stimulus, the action potential transitioned from the resting to the active state. The initial phase of activation, known as the threshold, was recorded at –58 mV, representing a 7 mV change required to initiate neuronal activation. Figure 1 illustrates the neuron's action potential and highlights the threshold voltage necessary to trigger depolarization. This 7 mV change served as the foundational parameter for the subsequent simulation results.

Simulations investigating the effect of varying the extracellular sodium (Na^+) concentration relative to the intracellular concentration revealed a relationship between the Na^+ and potassium (K^+) equilibrium potentials. The stimulus parameters were maintained at a pulse width of 0.1 ms and an amplitude of 65 μA, representing the normal action potential conditions illustrated in Figure 1. Under normal conditions, the Na^+ equilibrium potential was set at +50 mV and the K^+ equilibrium potential at –77 mV, corresponding to a normally activated neuron. When the Na^+ equilibrium potential was gradually reduced, the time interval between the threshold and depolarization phases increased. A reduction from +50 mV to +44 mV prolonged this interval, and further reduction to +43 mV resulted in a failure to depolarize, as shown in Figure 1. Under normal stimulation, the time from threshold to depolarization was approximately 0.89 ms (from 0.61 ms to 1.50 ms). However, reducing the Na^+ equilibrium potential to +44 mV extended this interval to 1.49 ms (from 0.61 ms to 2.10 ms), demonstrating the critical role of Na^+ in action potential dynamics. Conversely, increasing the extracellular Na^+ concentration beyond +50 mV, up to +360 mV, resulted in the skipping of the threshold phase altogether.

The simulation was then shifted to examine the effect of varying the potassium (K^+) equilibrium potential while maintaining the sodium (Na^+) equilibrium potential at +50 mV. Under normal neuronal activation, the K^+ equilibrium potential is –77 mV. Reducing the K^+ equilibrium potential to –71 mV resulted in failure of the action potential to depolarize. However, a slight reduction to –72 mV produced an action potential with a shortened time interval between threshold and depolarization, decreasing from 0.61 ms to 1.15 ms—a difference of 0.54 ms. Conversely, decreasing the K^+ equilibrium

potential to –79 mV also caused depolarization failure, while adjusting it to –78 mV led to a delay in depolarization onset. In this case, the threshold occurred at 0.61 ms, with depolarization initiating at 1.75 ms, resulting in a time difference of 1.14 ms between threshold and depolarization.

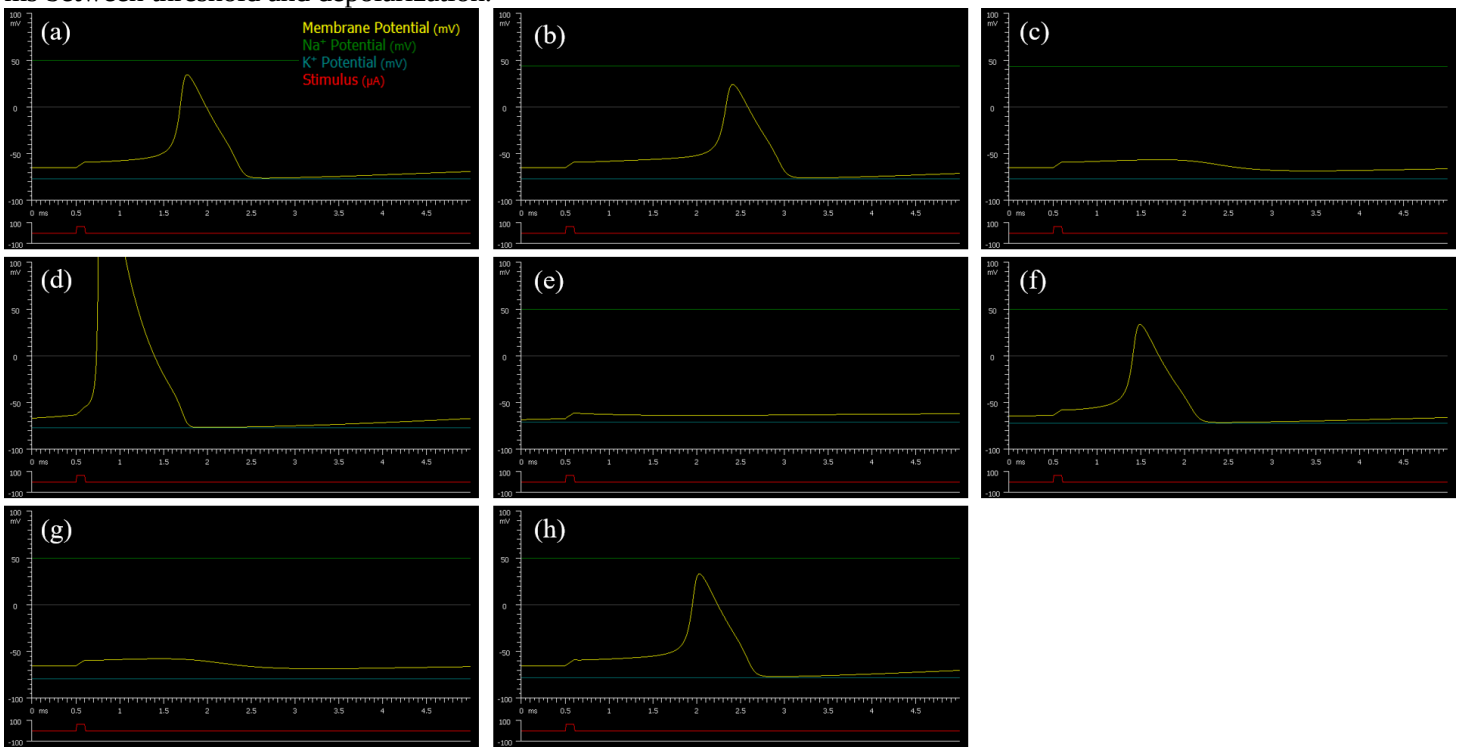

Fig. 1: (a) Neuron normal stimulation state. (b) Na^+ equilibrium at 44 mV. (c) Na^+ equilibrium at 43 mV. (d) Na^+ equilibrium at 360 mV. (e) K^+ equilibrium at -71 mV. (f) K^+ equilibrium at -72 mV. (g) K^+ equilibrium at -79 mV. (h) K^+ equilibrium at -78 mV.

3.2 Sensitivity recording

Sensitivity measurements were calculated using Equation 1, which relates voltage and pressure to determine sensitivity. Based on the laboratory transducer, the recorded voltage and pressure were 0.8 V and 860 kPa, respectively. Applying these values to Equation 1 yielded a sensitivity of S=0.8V/860Kpa=0.00000093 V/Pa.

3.3 Detection of thermal simulation

To validate our simulation experiments, the setup was aligned to mirror the actual therapeutic procedure used during High Intensity Focused Ultrasound (HIFU) treatment. The treatment delivered a power of 648 W and a total energy of 8,424 J; however, the intensity was not reported. To calculate the intensity, the area of the focused beam estimated to be 0.1457 cm^2 was used. Applying Equation 2, the intensity was determined as follows:

$$648 = (I)(0.1457) => I = \frac{648}{0.1457} = 4447.5\frac{W}{cm^2}$$

Also equals to $44{,}475{,}000\ \frac{\mathrm{W}}{\mathrm{cm}^2}$;

The corresponding pressure was calculated to be 12.03 MPa. This validation enabled us to proceed with the subsequent simulations. The intensity investigated was based on the neuronal threshold of 7 mV, resulting in a calculated pressure of 7,526 Pa, which corresponds to an intensity of 17.6 W/m^2 (0.00176 W/cm^2). The pressure calculation was performed using the first equation, as follows:

$$V = (P)(S) => P = \frac{V}{S} = \frac{0.007}{0.00000093} = 7526\ Pa$$

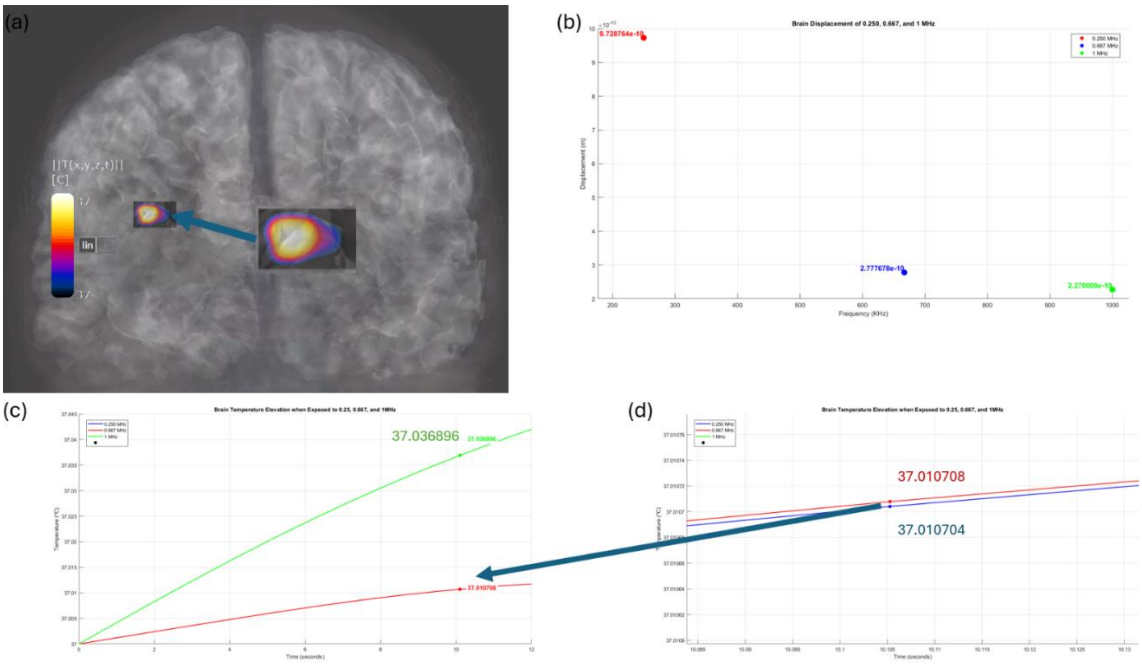

Fig. 2: (a) Temperature elevation profile for 1 MHz. (b) Brain displacement caused by frequencies of 0.250, 0.667, and 1MHz. (c) Temperature elevation caused by each frequency of 0.250, 0.667, and 1MHz. (d) Small temperature variation by 0.250, and 0.667 MHz

Table 2. Simulation result of temperature, displacement, force, and mechanical index

Frequency MHz	Temperature °C	Displacement nm	Force N/m^3	Mechanical Index
0.250	37.010704	0.971	0.03345	0.0138
0.667	37.010708	0.277	0.15052	0.00867
1	37.036869	0.227	0.16376	0.00727

Table 2 summarizes the effects of different ultrasound frequencies on brain tissue. As frequency increased, temperature elevation also increased, with a rise of 0.010704 °C at 0.250 MHz, 0.010708 °C at 0.677 MHz, and a higher temperature increase of 0.036869 °C at 1 MHz. These results demonstrate the impact of frequency on thermal effects.

Displacement decreased as frequency increased. At 0.250 MHz, the displacement measured 0.971 nm, which decreased to 0.277 nm at 0.677 MHz and further to 0.227 nm at 1 MHz.

Conversely, the force exerted increased with frequency: 0.03345 N/m³ at 0.250 MHz, 0.15052 N/m³ at 0.677 MHz, and 0.16376 N/m³ at 1 MHz.

The mechanical index (MI) decreased with increasing frequency, recording values of 0.0138 at 0.250 MHz, 0.00867 at 0.677 MHz, and 0.00727 at 1 MHz.

4.Discussion

When a neuron is stimulated from its resting membrane potential of –65 mV, activation of the action potential occurs as the membrane potential shifts to –58 mV. This 7 mV increase represents the threshold voltage required to transition the neuron from its resting to active state. Consequently, the simulations were based on this critical 7 mV voltage increase to model neuronal activation accurately.

Neuronal activity is primarily influenced by the concentrations of key ions, especially sodium (Na^+) and potassium (K^+). Variations in the extracellular-to-intracellular ratios of these ions can significantly alter neuronal behavior. Based on our

simulation results—conducted with a stimulus width of 0.1 ms and amplitude of 65 μA, and with Na^+ and K^+ equilibrium potentials initially set at +50 mV and –77 mV, respectively reducing the Na^+ equilibrium potential from +50 mV to +43 mV resulted in failure to reach the depolarization phase, suggesting neuronal inhibition at this ion ratio. At +44 mV, the time from threshold to depolarization was prolonged, increasing from 0.89 ms under normal conditions to 1.49 ms. These findings indicate that a lower extracellular Na^+ concentration lengthens the delay between threshold and depolarization and can ultimately inhibit neuronal activation. Conversely, increasing the Na^+ ratio accelerates depolarization; notably, at an elevated Na^+ equilibrium potential of +360 mV, the threshold phase was bypassed, leading to immediate action potential depolarization.

Simulation of varying potassium (K^+) equilibrium potentials revealed that increasing the potential from –77 mV to –71 mV resulted in failure of neuronal depolarization, indicating an inhibitory effect. Conversely, an increase to –72 mV allowed successful depolarization, with a reduced time from threshold to depolarization measured at 0.54 ms, which is shorter than the normal depolarization duration. When the K^+ equilibrium potential was decreased to –79 mV, action potential generation failed. At –78 mV, depolarization still occurred but with an increased delay, as the time from threshold to depolarization extended to 1.14 ms.

The calculated pressure based on the action potential threshold was 7.5 Pa, a relatively small value; however, it elicited varying brain responses depending on the frequency applied. Notably, temperature increased with rising frequencies, which may be related to frequency-dependent properties of brain tissue. Conversely, displacement decreased as frequency increased. This is likely due to the fact that lower frequencies have longer wavelengths, resulting in a wider focal area of influence. As frequency increases, the wavelength shortens, reducing both the affected area and the spatial separation between wavelengths. Additionally, the force exerted on the brain increased with frequency, indicating that higher frequencies impart greater mechanical forces. Since the mechanical index (MI) depends on frequency and safety concerns typically arise at values above 0.4, all frequencies tested at the threshold pressure were well within safe limits.

5.Conclusion

To our knowledge, this study presents the first in silico framework integrating biophysical neuron models with focused ultrasound acoustic and thermal simulations by converting neuronal threshold voltage into equivalent pressure values. This integrated simulation approach enables detailed investigation of the mechanical and thermal effects of ultrasound on neuronal activation with high spatial precision.

While the simulation framework demonstrates significant strengths in modeling neuron-ultrasound interactions, it has limitations. In particular, MetaNeuron does not currently simulate neuronal responses to mechanical ultrasound exposure, and the approach would benefit from experimental validation to fully assess its predictive accuracy. Nonetheless, this work lays a critical foundation for optimizing ultrasound parameters for safe and effective non-invasive neuromodulation, potentially advancing clinical therapies for neurological conditions and research.

Acknowledgements

The author would like to thank Sim4Life for the usage of their simulation software for acosutic and thermal simulation. The authour would also like to thank Univeristy of Dundee and York to make the work possible.

References

[1] Z.-D. Deng, S. H. Lisanby, and A. V. Peterchev, “Electric field depth–focality tradeoff in transcranial magnetic stimulation: Simulation comparison of 50 coil designs,” *Brain Stimulation*, vol. 6, no. 1, pp. 1–13, Jan. 2013, doi: https://doi.org/10.1016/j.brs.2012.02.005.

[2] A. Datta, V. Bansal, J. Diaz, J. Patel, D. Reato, and M. Bikson, “Gyri-precise head model of transcranial direct current stimulation: Improved spatial focality using a ring electrode versus conventional rectangular pad,” *Brain Stimulation*, vol. 2, no. 4, pp. 201-207.e1, Oct. 2009, doi: https://doi.org/10.1016/j.brs.2009.03.005.

[3] Robert and G. F. Woodman, “Enhancing long-term memory with stimulation tunes visual attention in one trial,” *Proceedings of the National Academy of Sciences of the United States of America*, vol. 112, no. 2, pp. 625–630, Dec. 2014, doi: https://doi.org/10.1073/pnas.1417259112.
[4] L. Mencarelli, A. Menardi, F. Neri, L. Monti, G. Ruffini, R. Salvador, A. Pascual-Leone, D. Momi, G. Sprugnoli, A. Rossi, S. Rossi, E. Santarnecchi, “Impact of network-targeted multichannel transcranial direct current stimulation on intrinsic and network-to-network functional connectivity,” *Journal of Neuroscience Research*, vol. 98, no. 10, pp. 1843–1856, Jul. 2020, doi: https://doi.org/10.1002/jnr.24690.
[5] J. Dell’Italia, J. L. Sanguinetti, M. M. Monti, A. Bystritsky, and N. Reggente, “Current State of Potential Mechanisms Supporting Low Intensity Focused Ultrasound for Neuromodulation,” *Frontiers in Human Neuroscience*, vol. 16, Apr. 2022, doi: https://doi.org/10.3389/fnhum.2022.872639.
[6] P.-C. Zhang, A. M. Keleshian, and F. Sachs, “Voltage-induced membrane movement,” *Nature*, vol. 413, no. 6854, pp. 428–432, Sep. 2001, doi: https://doi.org/10.1038/35096578.
[7] J. K. Mueller and W. J. Tyler, “A quantitative overview of biophysical forces impinging on neural function,” vol. 11, no. 5, pp. 051001–051001, Aug. 2014, doi: https://doi.org/10.1088/1478-3975/11/5/051001.
[8] D. P. Darrow, P. O’Brien, T. J. Richner, T. I. Netoff, and E. S. Ebbini, “Reversible neuroinhibition by focused ultrasound is mediated by a thermal mechanism,” *Brain Stimulation*, vol. 12, no. 6, pp. 1439–1447, Nov. 2019, doi: https://doi.org/10.1016/j.brs.2019.07.015.
[9] “Welcome | MetaNeuron,” *www.metaneuron.org*. https://www.metaneuron.org/
[10] “Sim4Life,” *sim4life*, 2025. https://sim4life.swiss/
[11] M. W. Barnett and P. M. Larkman, “The action potential,” *Practical Neurology*, vol. 7, no. 3, pp. 192–197, Jun. 2007, Available: https://pn.bmj.com/content/7/3/192
[12] “Precision Acoustics - Ultrasound Acoustics,” *Precision Acoustics*. https://www.acoustics.co.uk/
[13] J. Gümmer, S. Schenke, and F. Denner, “Modelling Lipid-Coated Microbubbles in Focused Ultrasound Applications at Subresonance Frequencies,” *Ultrasound in Medicine & Biology*, vol. 47, no. 10, pp. 2958–2979, Oct. 2021, doi: https://doi.org/10.1016/j.ultrasmedbio.2021.06.012.
[14] T. R. Wang, A. E. Bond, R. F. Dallapiazza, A. Blanke, D. Tilden, T. E. Hureta, S. Moosa, F. U. Prada, W. J. Elias, “Transcranial magnetic resonance imaging–guided focused ultrasound thalamotomy for tremor: technical note,” *Neurosurgical Focus*, vol. 44, no. 2, p. E3, Feb. 2018, doi: https://doi.org/10.3171/2017.10.focus17609.